Progress In Electromagnetics Research C, Vol. 61, 27–35, 2016

X-Band Aperture Antenna with Hybrid Dielectric Inserts

Igor Ivanchenko[1], Maksym Khruslov[1], Vadim Plakhtiy[1], Nina Popenko[1], and Daniel Rönnow[2, *]

Abstract—An X-band radiator as an open-ended waveguide with a hybrid dielectric insert is proposed. The insert is in the form of a parallelepiped, which fills the entire cross section of the waveguide and constitutes a Teflon matrix with local inhomogeneities in the form of dielectric cylinders with a different permittivity. The design allows for forming various near-field distributions and, hence, the radiator performance by means of definite combinations of the local inhomogeneities can be modified. A number of configurations in the location of air and quartz cylinders are investigated. The calculated and experimental results are in good agreement. The proposed approach to the near-field formation of the aperture antenna is promising, because the variety of possible configurations in the location of local inhomogeneities with different permittivity provides new opportunities in terms of designing both single radiators and antenna arrays.

1. INTRODUCTION

Aperture radiators based on rectangular waveguides are widely used in microwave technology, both as individual antennas and phased arrays with close packing of elements and wide-angle scanning when operating at high levels of microwave power. In this respect, there is a need to reduce the cross-section of the elements. Open-ended waveguides filled with a dielectric are commonly used as transceiver probes or antennas. The problem of waveguide matching with the free space becomes the main design problem for this type of antennas. Different techniques for matching the antenna to its feeding line have been reported in the literature [1–3]. In particular, in [1] good matching is achieved by using an additional matching layer with lower permittivity. An alternative technique is the use of air gaps between dielectric filling elements in the waveguide to achieve high performance of both the individual radiator and the array itself; this technique has been used in the frequency range 1–3 GHz [2, 3]. There are also several types of probe design [4–7] for measuring the near-field distribution in the microwave and millimeter wave ranges. Near-field microwave probes have been extensively used in non-destructive testing. For example, in [8] a layered medium at the end of an open-ended waveguide was used for improved sensitivity. In [9] the original approach to the problem of antenna-probe miniaturization for the precision EM field measurements is presented. Recently, metamaterials have been used to achieve improved near-field properties [10, 11]. The used metamaterials consist of split ring resonators or similar metallic structures. Similar metamaterials have also been used to achieve improved directivity of the far field properties of the open-ended antennae [12, 13].

Turning to the antenna technology, it should be noted that an underwater open ended waveguide antenna for the 2.4 GHz industrial, scientific, and medical band is presented in [14]. An antenna array consisting of dielectrically filled open-ended waveguides with an original type of array excitation and the wide-angle beam steering is presented in [15]. A compact antenna based on an open-ended rectangular

Received 1 September 2015, Accepted 16 December 2015, Scheduled 29 December 2015

* Corresponding author: Daniel Rönnow (daniel.ronnow@hig.se).

[1] O. Ya. Usikov Institute for Radiophysics and Electronics of the NAS of Ukraine, Ukraine. [2] Department of Electronics, Mathematics and Natural Sciences, University of Gävle, SE-801 76 Gävle, Sweden.

waveguide structure with a bowtie feeding structure, which efficiently excites the fundamental mode and allows the use of near-field wire grid polarizer to further improve the cross-pol antenna, is proposed in [16] to obtain good antenna performance in the band 1.08–4.9 GHz. A promising technology for compact structures is the substrate integrated waveguide (SIW) technology which allows a non planar structure like a horn antenna to be transformed into a planar form. In [17] a rectangular dielectric loaded SIW H-plane sectoral horn antenna was designed for operating at various frequencies in the range 21–28 GHz, which makes it a good candidate for automotive radar applications.

In the present study we use dielectric rods in a dielectric matrix to modify the near-field of an open-ended waveguide. The structure is similar to the one reported in [18], in which dielectric rods in a dielectric matrix were used to get left handedness in the X-band. To our knowledge the type of all dielectric structures that we report has not been used for modifying near-field properties of open-ended waveguides. We propose an antenna based on an open-ended waveguide filled with a hybrid dielectric insert that enables the forming of various near-field distributions. By using inserts like those that we propose, it is possible to design a number of antennas of this class with a variety of radiation characteristics by various modifications of the insert configuration (the change in the period of the lattice formed by the local inhomogeneities, the number of rows of the lattice, the relative permittivity of inhomogeneities, their topology, etc.).

2. ANTENNA DESIGN

The proposed antenna design is an open-ended waveguide, 1, with the hybrid dielectric insert, 2, inside. The latter consists of a dielectric matrix, 3, in which the local inhomogeneities, 4, of cylindrical shape are equidistantly located (Fig. 1(a)). The cross-section of the dielectric matrix, 3, corresponds to the cross-section of the waveguide, and the size of the matrix along the x-axis is 10 mm. Dielectric cylinders of diameter d form the double-row lattice with the distance l between the rows (Fig. 1(b)). The number of cylinders in each row is 7, so that the distance between their axes is 2.9 mm. The permittivity of the cylinder's material and the matrix differ from each other. The axes of all cylinders were oriented parallel to the vector $\mathbf{E}$ of the operational mode H_{01} in the waveguide. In the process of simulations the following parameters were varied: 1) the diameter of cylinders ($0.5\,\text{mm} < d < 1.5\,\text{mm}$), 2) the lattice period ($3\,\text{mm} < l < 7\,\text{mm}$), and 3) the permittivity of cylinders ($1 < \varepsilon_1 < 10$) located in the Teflon matrix with $\varepsilon = 2.04$.

The parameter S_{11}, radiation pattern, and near-field distributions were simulated by using ANSYS HFSS software. A number of antenna designs with different combinations of dielectric cylinders with the different permittivity are analyzed. Some of them have been manufactured and tested in the frequency band 8–12 GHz. A photograph of an antenna element with one of the dielectric insert configurations is shown in Fig. 2. The frequency dependence of the parameter S_{11} was measured using a Rodhe & Schwarz Vector Network Analyzer ZVB14. Radiation pattern measurements were carried out in an anechoic chamber using the equipment described in [19]. In this case, the accuracy in the position of the receiving horn antenna and in the operational frequency was $\pm 0.5^\circ$ and ± 8 MHz, respectively.

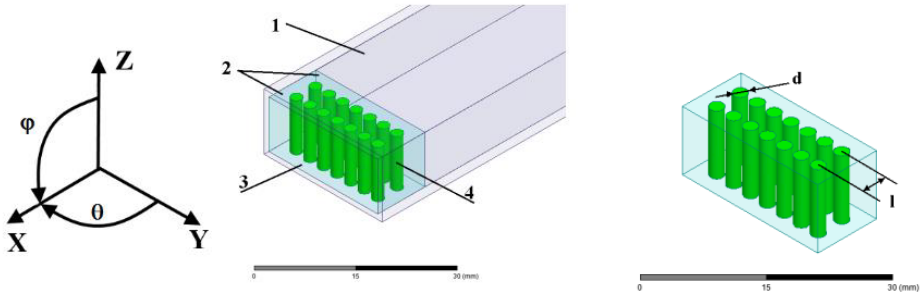

(a) (b)

Figure 1. (a) The open-ended waveguide and (b) the configuration of dielectric insert.

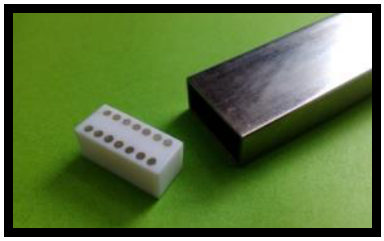

Figure 2. Photograph of an antenna element.

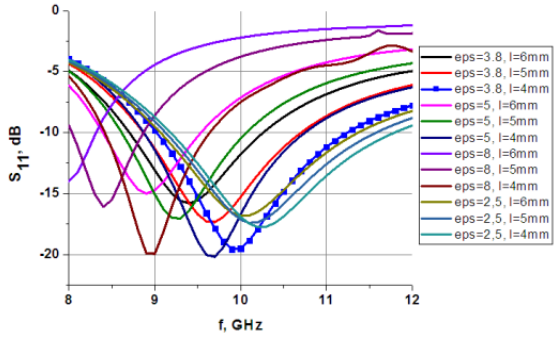

Figure 3. Simulated parameter S_{11}.

3. ANALYSIS OF RESULTS

3.1. Design 1

First of all we have performed the simulations of the parameter S_{11} varying the permittivity and the lattice period of cylinders. The results of the simulations are shown in Fig. 3. The dotted curve ($\varepsilon_1 = 3.8$, $l = 4$) was selected as the best one. For the **Design 1** all the cylinders used have the permittivity $\varepsilon_1 = 3.8$.

The simulation results of an antenna in the case when all the cylinders in the Teflon matrix are made of fused quartz ($\varepsilon = 3.8$) are summarized in Fig. 4. The near-field distribution is symmetrical, see Fig. 4(a), and the resonant frequency $f_r = 10\,\text{GHz}$. The simulated $-10\,\text{dB}$ impedance bandwidth $\Delta f = 2.3\,\text{GHz}$ (Fig. 4(b)). In this case the measured antenna bandwidth is equal to $\Delta f = 2.1\,\text{GHz}$. As one sees from the Fig. 4(b), the measured input return loss has a difficult rugged view associated with poor antenna matching in the experiment. Indeed, it is well known that the placement of a dielectric inside the waveguide always violates the conditions of the waveguide channel matching, resulting in a complex frequency dependence of the parameter S_{11}. Therefore, in practice special efforts are made to optimize the matching conditions in each specific case. In the framework of this research we have shown that without any additional measures one can find the conditions of the best wave impedance matching by moving the dielectric insert inside the waveguide. Furthermore, the observed shift in the parameter S_{11} which is seen when comparing the measured and simulated results can be explained by the fact that our simulations were made for a single-mode case, which may give systematic errors. Since the effect of these errors is the same for all simulated structures, the comparison with different structures is still relevant.

This antenna produces symmetric radiation patterns in the two principal planes (Figs. 4(c), (d)). The simulated beamwidths at the $-3\,\text{dB}$ power level in the E- and H-planes are $\Delta\theta = 105°$ and $\Delta\theta = 62°$, respectively. It is worth noting that the measured radiation pattern in the H-plane is wider than the simulated one and its width amounts to $\Delta\theta = 76°$. The discrepancy in the radiation pattern widths may be due to differences between the actual and calculated dielectric constant of the elements, which form a dielectric insert, as well as the neglect in calculations of the diffraction of EM waves by the final thickness of waveguide walls. The effect of that will be more pronounced in the radiation pattern formation in the H-plane in accordance with the polarization of the EM wave in the waveguide for the H_{10} mode.

We have found that the antenna matching can be controlled by changing the location of the insert in the waveguide. The antenna characteristics are improved when we pull out the insert relative to the open-ended waveguide aperture. Fig. 5(a) shows the frequency dependence of the S_{11} parameter when the insert is displaced by $L = 3.3\,\text{mm}$. In this case, the antenna bandwidth corresponds to the estimated one ($\Delta f = 2.3\,\text{GHz}$). At the same time, the displacement of the insert into the waveguide is accompanied by the antenna mismatch and gradual narrowing the antenna bandwidth. Figs. 5(b) and 5(c) illustrate the parameter S_{11} of the antenna at two fixed insert locations. For these two cases the antenna bandwidth is $\Delta f = 2.16\,\text{GHz}$ for $L = -1.4\,\text{mm}$ and $\Delta f = 2.12\,\text{GHz}$ for $L = -3.4\,\text{mm}$. As can

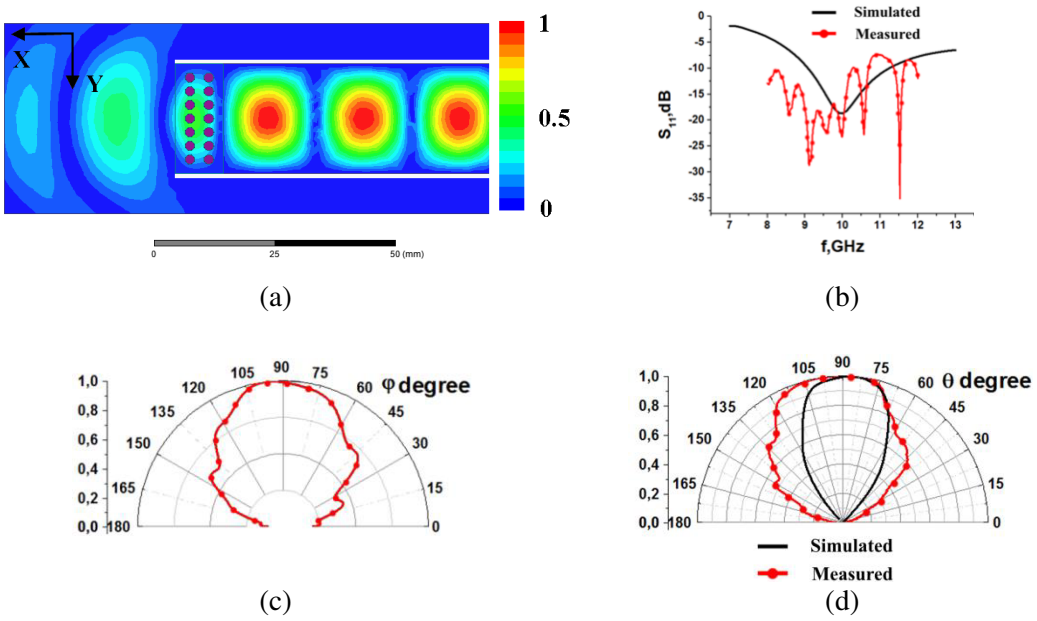

Figure 4. (a) Near-field distribution; (b) simulated and measured parameter S_{11}; the radiation patterns in the two principal planes: (c) E-plane — measured, and (d) H-plane at the resonant frequency $f_r = 10\,\text{GHz}$.

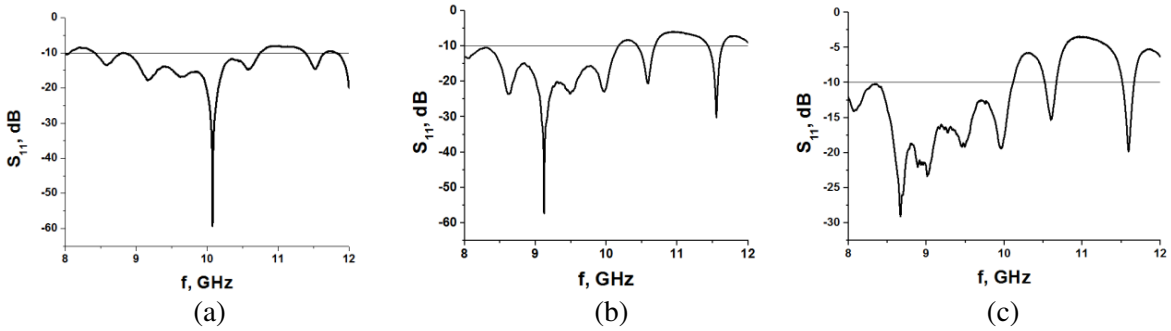

Figure 5. Measured S_{11} parameter of the antenna with different insert positions: (a) $L = 3.3\,\text{mm}$ ($f_r = 10.1\,\text{GHz}$); (b) $L = -1.4\,\text{mm}$ ($f_r = 9.12\,\text{GHz}$); (c) $L = -3.4\,\text{mm}$ ($f_r = 8.65\,\text{GHz}$).

be seen, the resonant frequency, f_r, of the antenna depends also upon the insert position relative to the open-ended waveguide aperture. The corresponding resonant frequencies for the three aforementioned cases are shown in the figure caption. The input return loss at the symmetrical insert positions with respect to the open-ended waveguide aperture (Fig. 5(a) and Fig. 5(c)) demonstrates the significantly different form of these dependences. However, the radiation pattern retains its own shape within the antenna bandwidth and the elevation angle of peak directivity corresponds to zenith.

The mutual combination of cylinders with different permittivity in the hybrid insert leads to a substantial changing in the antenna performance. Different configurations of the two-row lattice of dielectric cylinders were analyzed, as described in the following.

3.2. Design 2

In this case all the cylinders have a lower effective permittivity $\varepsilon = 1$, and simulation results are shown in Fig. 6. The near-field picture, Fig. 6(a), shows a better antenna matching with the free space resulting in increased antenna bandwidth, which exceeds 3 GHz (Fig. 6(b)). The resonant frequency of

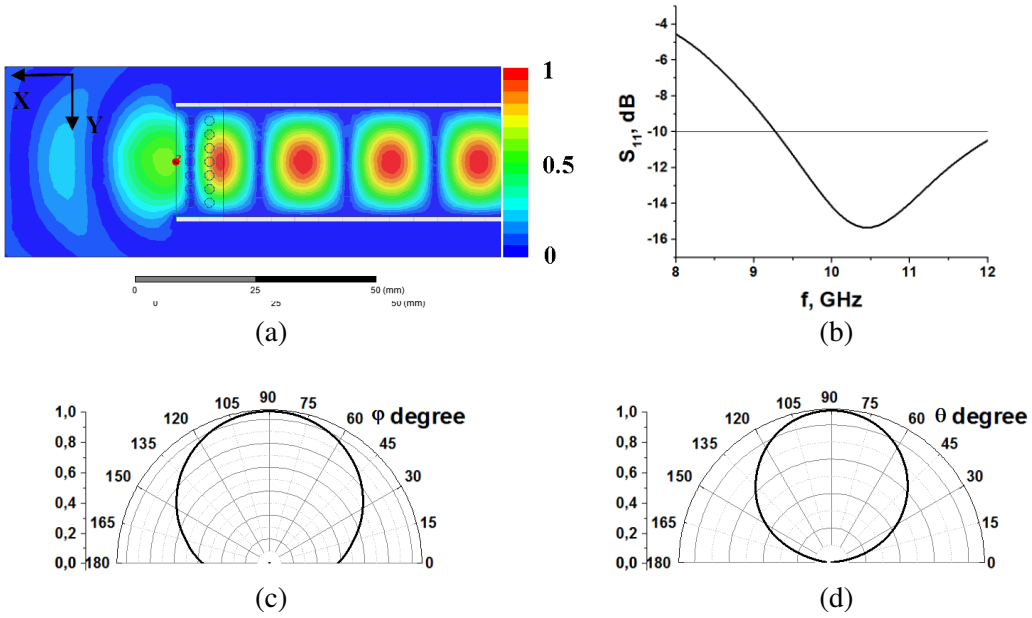

Figure 6. (a) Near-field distribution; (b) simulated parameter S_{11}; the radiation patterns in the (c) E- and (d) H-planes.

this an antenna is shifted towards higher frequencies and equals to $f_r = 10.5\,\text{GHz}$. We can see the axial antenna radiation in both principal planes (Figs. 6(c), (d)) but their beamwidths differ and are equal to $\Delta\theta = 106^\circ$ in the E-plane and $\Delta\theta = 76^\circ$ in the H-plane. Thus, the use of the lower effective insert permittivity gives rise to beamwidth enlargement in the H-plane.

3.3. Design 3

Figure 7 shows the simulated antenna characteristics in the case of the lattice configuration shown in Fig. 7(a). Here, the light circles correspond to the air and the dark circles correspond to the quartz. The near-field distribution of the antenna ceases to be symmetrical due to different reflection coefficients of the operation waveguide mode in the upper and lower areas of the waveguide (Fig. 7(a)). For a lattice configuration like that the waveguide matching with free space in the lower area of the waveguide is better due to more gradual increase in the insert permeability from the waveguide to the free space. As a result, it leads to the enlargement in the $-10\,\text{dB}$ impedance bandwidth of more than 40% ($\Delta f > 3.7\,\text{GHz}$) in comparison with **Design 1** (see Fig. 4(b) and Fig. 7(b)) and to the definite near-field transformation (Fig. 7(a)). The resonant frequency of the antenna is shifted towards lower frequencies, $f_r = 9.8\,\text{GHz}$. A comparison of this antenna design with the **Design 1** gives that the radiation pattern in both principal planes is significantly narrowed and is equal to $\Delta\theta = 64^\circ$ in the E-plane (Fig. 7(c)) and $\Delta\theta = 49^\circ$ in the H-plane (Fig. 7(d)), where we can observe the rotation in the elevation angle of peak directivity at $\varphi = +15^\circ$ relative to zenith ($\varphi = 90^\circ$).

3.4. Design 4

The other lattice configuration, in which two quartz cylinders are used in the left row of the lattice instead of three ones as for the **Design 3,** is shown in the Fig. 8(a). Such a change in the lattice topology gives rise to some narrowing in the antenna bandwidth ($\Delta f = 3.17\,\text{GHz}$), as seen in Fig. 8(b), compared with the **Design 3** while the resonant frequency $f_r = 10.0\,\text{GHz}$ corresponds to **Design 1.** The measurements on such an antenna showed that in analogy with the **Design 1** the antenna bandwidth does not reach the simulated value and is equal to $\Delta f = 2.43\,\text{GHz}$. The resonant frequency is shifted towards lower frequencies with $\sim 300\,\text{MHz}$. It is worth mentioning that in Fig. 8(b) the ripples in the measured input return loss are much less than for **Design 1** (Fig. 4(b)).

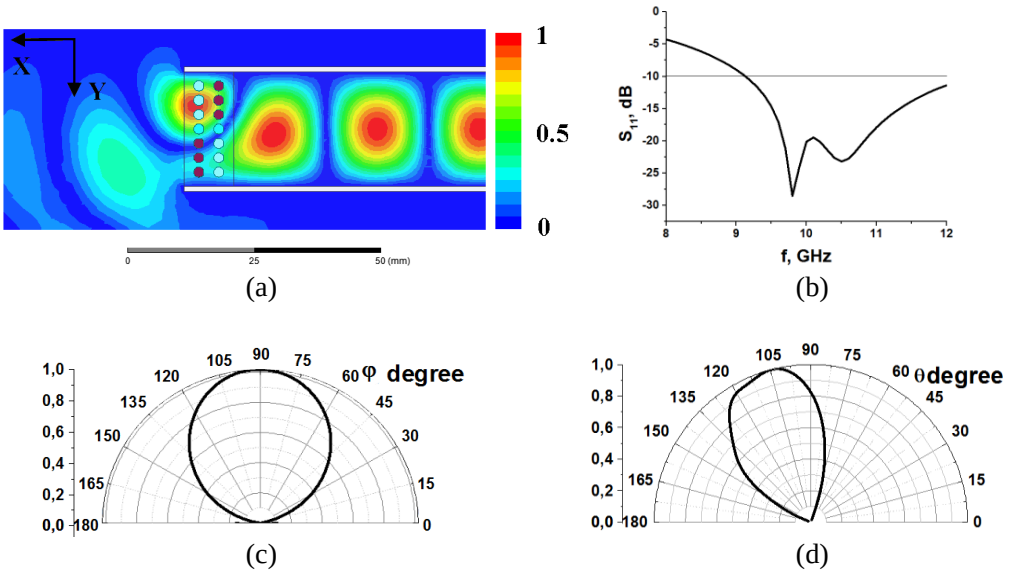

Figure 7. (a) Simulated near-field distribution; (b) S_{11} parameter; the radiation patterns in the (c) E- and (d) H-planes at the resonant frequency $f_r = 9.8\,\text{GHz}$.

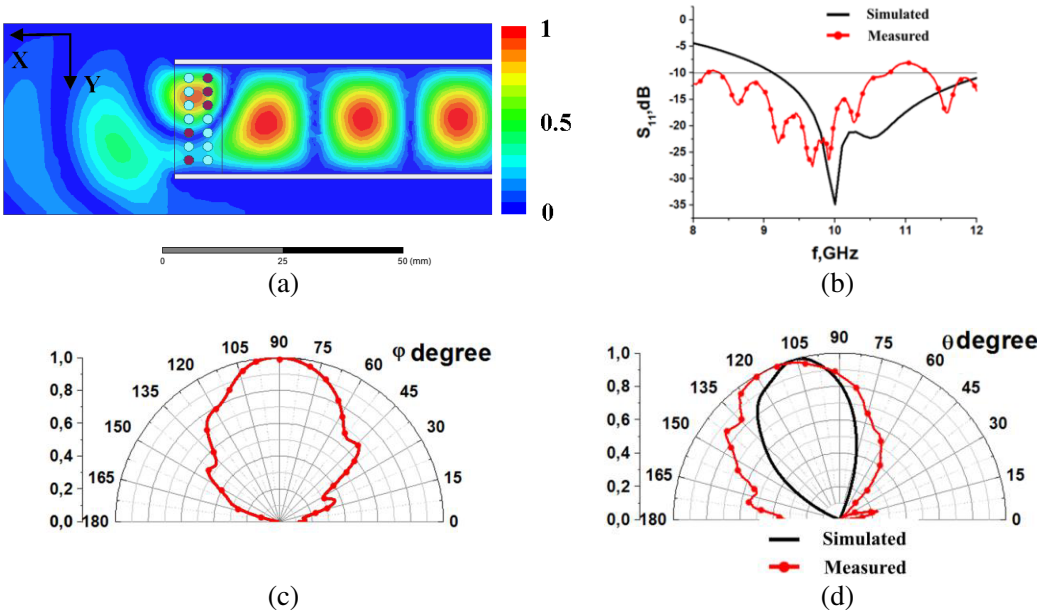

Figure 8. (a) Near-field distribution; (b) simulated and measured parameter S_{11}; the radiation patterns in two principal planes: (c) E-plane — measured, and (d) H-plane at the resonant frequency $f_r = 10\,\text{GHz}$.

A comparative analysis of **Design 4** and **Design 3** shows that both antennas radiate in zenith in the E-plane, but the beamwidth of **Design 4** is broader ($\Delta\theta = 74°$ compared to $\Delta\theta = 64°$), as seen in Fig. 8(c) and Fig. 7(c). At the same time, in the H-plane the simulated beamwidth remains virtually the same as for **Design 3** ($\Delta\theta = 46°$ and $\Delta\theta = 49°$, respectively) while the measured radiation pattern width is wider than the simulated one (Fig. 8(d)) and amounts to $\Delta\theta = 72°$. In the experimental data we can observe the rotation of the elevation angle of peak directivity at $\varphi + 23°$ relative to zenith compared with the simulated value $\varphi = +15°$, Fig. 8(d).

The disagreement between simulated and measured results in Figs. 8(b), (d) is explained by the same factors that have been noted above and relating to Figs. 4(b), (d). It is worth noting that the accuracy of the measured radiation patterns in both principal planes does not exceed 1°.

3.5. Design 5

The change in lattice topology by a mirror operation with respect to the **Design 4** results, naturally, in the mirror reflection of the near-field pattern (Fig. 9(a)) and the rotation of the elevation angle of peak directivity in the opposite direction at $\varphi = -15°$ from zenith **4** (compare Fig. 8(d) and Fig. 9(b)). All the other characteristics of the antenna remain unchanged.

3.6. Design 6

Finally, we have examined one more of the possible lattice topologies (Fig. 10(a)). In the simulation results, one can see a slight distortion of the near-field distribution in the vicinity of the quartz cylinders. Such a field transformation leads to a small rotation ($\varphi \approx +7°$) of the elevation angle of peak directivity relative to the antenna axis in the H-plane (Fig. 10(d)). However, the other characteristics of the antenna exhibit large changes; the radiation pattern becomes very broad in both principal planes,

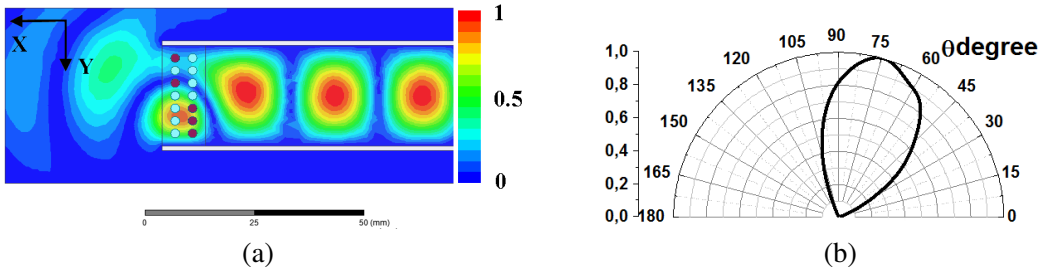

(a) (b)

Figure 9. (a) Simulated near-field distribution and (b) radiation pattern in the H-plane.

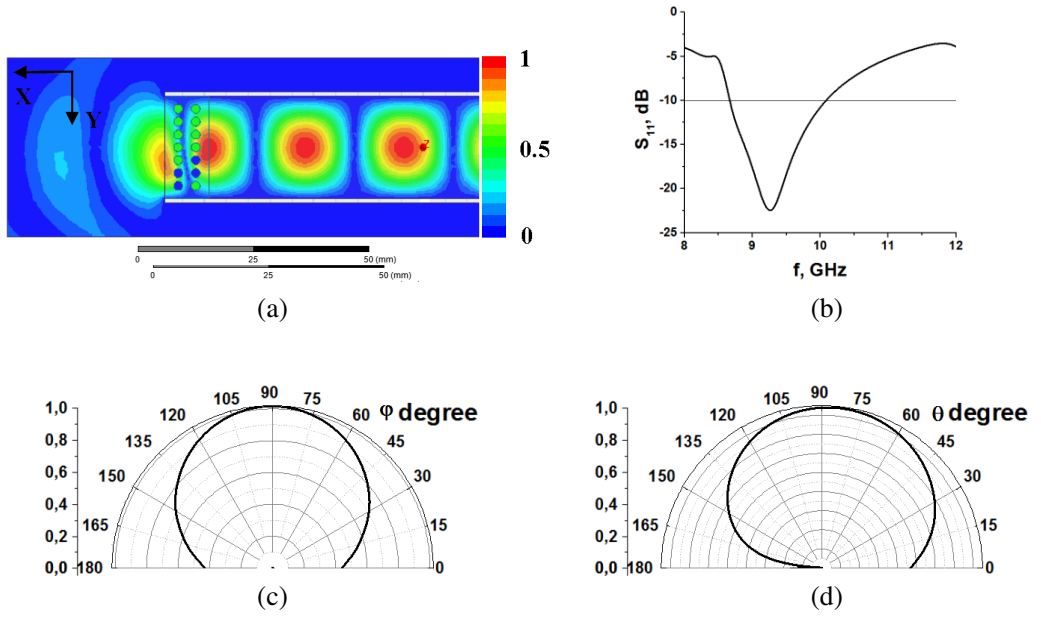

(a) (b)

(c) (d)

Figure 10. (a) Simulated near-field distribution; (b) S_{11}; radiation patterns (c) in the E-plane and (d) in the H-plane.

$\Delta\theta = 120^\circ$ in the E-plane and $\Delta\theta = 101^\circ$ in the H-plane, respectively, while the antenna bandwidth is largely narrowed and is $\Delta f = 1.35\,\mathrm{GHz}$ (Fig. 10(b)).

4. CONCLUSIONS

In this paper aperture X-band antennas as open-ended waveguides with a hybrid dielectric insert with local inhomogeneities of the dielectric cylinders with different permittivity (air and quartz) are proposed. The findings demonstrate the possibility to control the near-field distribution and hence the antenna performance by means of specific combinations of the dielectric cylinders permittivity and are as follows:

- Symmetrical (with respect to the waveguide axis) location of the quartz and air cylinders leads to broadening of the operational frequency band ($\Delta f > 3.7\,\mathrm{GHz}$) compared with the homogeneous lattice and causes a beam steering of the radiation pattern in the H-plane.
- Non-symmetrical location of the quartz and air cylinders (with respect to the waveguide axis) allows one to obtain radiation patterns with practically the same beamwidth in the H- and E-planes, but in a narrower frequency band ($\Delta f = 1.35\,\mathrm{GHz}$).
- The change of the insert position relative to the antenna aperture enables broadening of the operational frequency band by more than 18%.

Thus, the proposed approach to the near-field formation of aperture antennas as the open-ended waveguide filled with an artificial dielectric is promising; the high number of possible combinations of the location of local inhomogeneities with different ε inside the original dielectric matrix provides new opportunities both in terms of designing the single radiators and antenna arrays.

REFERENCES

1. Lee, J. J. and R.-S. Chu, "Aperture matching of a dielectric loaded circular waveguide element array," *IEEE Trans. Antennas Propag.*, Vol. 37, 395–399, 1989.
2. Coman, C. I., I. E. Lager, and L. P. Ligthart, "The design of a matching circuit for dielectric-filled open-ended waveguide antenna," *Proc. European Radar Conf.*, 1409–1412, 2004.
3. Coman, C. I., I. E. Lager, and L. P. Ligthart, "Optimization of linear sparse array antennas consisting of electromagnetically coupled apertures," *Proc. European Radar Conf.*, 302–304, 2004.
4. Gardiol, F. and J.-C. Bolomey, *Engineering Applications of the Modulated Scatterer Technique*, Artech House, Boston, 2001.
5. Bakhtiari, S., S. I. Ganchev, and R. Zoughi, "Open-ended rectangular waveguide for nondestructive thickness measurement and detection of lossy dielectric slabs backed by a conductive plate," *IEEE Trans. Intrum. Meas.*, Vol. 42, 19–24, 1993.
6. Maazi, M., D. Glay, and T. Lasri, "Millimeter wave non destructive technologies and artificial neural networks for near field characterization of embedded defects," *Proc. ICONIC 2005*, 329–334, 2005.
7. Chernobrovkin, R., I. Ivanchenko, and N. Popenko, "A novel V-band antenna for nondestructive testing techniques," *Microw. Opt. Techn. Lett.*, Vol. 49, No. 7, 1732–1735, 2007.
8. Qaddoumi, N. Q., W. M. Saleh, and M. Abou-Khousa, "Innovative near-field microwave nondestructive testing of corroded metallic structures utilizing open-ended rectangular waveguide probes," *IEEE Trans. Intrum. Meas.*, Vol. 56, 1961–1966, 2007.
9. Chernobrovkin, R., I. Ivanchenko, and N. Popenko, "A novel V-band antenna for nondestructive testing techniques," *Microw. Opt. Techn. Lett.*, Vol. 49, No. 7, 1732–1735, 2007.
10. Yang, J. J., M. Huang, H. Tang, J. Zeng, and L. Dong, "Metamaterial sensors," *Int. J. Antennas Propag.*, Vol. 2013, Article ID 637270, 2013.
11. Ren, Z., S. B. Muhammed, and O. M. Ramahi, "Near-field subsurface detection using metamaterial inspired probes," *Appl. Phys. A*, Vol. 103, 839–842, 2011.
12. Hwang, R.-B., H.-W. Liu, and C.-Y. Chin, "A metamaterial-based E-plane horn antenna," *Progress In Electromagnetics Research*, Vol. 93, 275–289, 2009.

13. Tomaz, A., J. J. Barroso, U. C. Hasar, and A. J. Faro Orlando, "Directivity enhancement of an X-band horn antenna loaded by a wire medium," *PIERS Proceedings*, 1128–1131, Stockholm, August 12–15, 2013.
14. Sporer M., A. Friedrich, R. Weigel, and A. Koelpin, "Open-ended dielectric-filled waveguide antenna for underwater usage," *European Microwave Conference (EuMC) 2014*, 1683–1686, 2014.
15. Chernobrovkin, R., I. Ivanchenko, L. Ligthart, A. Korolev, and N. Popenko, "Wide-angle X-band antenna array with novel radiating elements," *Radioengineering*, Vol. 17, No. 2, 72–76, 2008.
16. Elsherbini, A. and K. Sarabandi, "Compact directive ultra-wideband rectangular waveguide based antenna for radar and communication applications," *IEEE Trans. Antennas Propag.*, Vol. 60, No. 5, 2203–2209, 2012.
17. Ranade S. R. and D. U. Nair, "Design of a substrate integrated waveguide H plane horn antenna on a PTFE substrate for automotive radar application," *Applied Electromagnetics Conference (AEMC), 2011 IEEE*, 1–4, 2011.
18. Wang, J., Z. Xu, Z. Yu, X. Wei, Y. Yang, J. Wang, and S. Qu, "Experimental realization of all-dielectric composite cubes/rods left-handed metamaterial," *J. Appl. Phys.*, Vol. 109, 084918, 2011.
19. Andrenko, A. S., I. V. Ivanchenko, D. I. Ivanchenko, S. Y. Karelin, A. M. Korolev, E. P. Laz'ko, and N. A. Popenko, "Active broad X-band circular patch antenna," *IEEE Antennas Wireless Propag. Lett.*, Vol. 5, 529-533, 2006.